Results in Physics 9 (2018) 1044–1049

Contents lists available at ScienceDirect

Results in Physics

journal homepage: www.elsevier.com/locate/rinp

Modeling optical transmissivity of graphene grate in on-chip silicon photonic device

Iraj S. Amiri[a,b,*], M.M. Ariannejad[c], M.A. Jalil[d], J. Ali[e], P. Yupapin[a]

[a] Computational Optics Research Group, Advanced Institute of Materials Science, Ton Duc Thang University, Ho Chi Minh City, Viet Nam
[b] Faculty of Applied Sciences, Ton Duc Thang University, Ho Chi Minh City, Viet Nam
[c] Photonics Research Centre, University of Malaya, 50603 Kuala Lumpur, Malaysia
[d] Physics Department, Faculty of Science, Universiti Teknologi Malaysia, 81310 Johor Bahru, Malaysia
[e] Laser Center, Ibnu Sina Institute for Industrial and Scientific Research, Universiti Teknologi Malaysia, 81300 Johor Bahru, Malaysia

ARTICLE INFO

Keywords:
Optical waveguide
Silicon waveguide
Grate
Graphene
Optical transmissivity

ABSTRACT

A three-dimensional (3-D) finite-difference-time-domain (FDTD) analysis was used to simulate a silicon photonic waveguide. We have calculated power and transmission of the graphene used as single or multilayers to study the light transmission behavior. A new technique has been developed to define the straight silicon waveguide integrated with grate graphene layer. The waveguide has a variable grate spacing to be filled by the graphene layer. The number of graphene atomic layers varies between 100 and 1000 (or 380 nm and 3800 nm), the transmitted power obtained varies as ~30% and ~80%. The ~99%, blocking of the light was occurred in 10,000 (or 38,000 nm) atomic layers of the graphene grate.

Introduction

Applications for photonic integrated circuits from fiber-optic communication to biomedical sensing and photonic computing are possible [1–5]. Graphene is a two-dimensional material with a honeycomb structure and has unique physical, mechanical, and electrical properties [6,7]. For photonics applications, graphene is highly desirable due to significant optical and electrical properties, where it has been utilized in compatible material systems [8–11]. Graphene has been used in optical systems due to owing ultra-wideband absorption, easily adjustable inter-band transitions, having high carrier mobility and showing highly stable nonlinear absorption [12–18]. High-quality graphene can be produced at wafer scales and transferred to the heterogeneous substrates, where it can be patterned into the planar waveguide devices for the optoelectronic semiconductor applications [7,19–22]. Combinations of graphene and silicon in compatible photonics system are highly desired for the high speed-low power integrated photonics systems with complementary metal oxide semiconductor (CMOS) circuits [23,24]. Several semiconductor devices and also graphene-based devices have been demonstrated recently, including polarization controllers [25], ultra-fast pulsed lasers [26], resonators [27–29] and optical filters [30].

The investigation of optical properties of graphene has been performed using free-space optics with normal incident configurations in many research works such as in the reference [31]. Graphene is a two-dimensional material and it is considered as foundational material for the optoelectronic devices and CMOS integrated systems [10,32]. For the application of electro-absorption modulation, saturable absorption and also the polarization conversion, long interaction length of graphene is essential. This can be provided by integrating graphene with planner waveguides or optical fibers. In this case, the interaction length of the graphene can be limited by the length of the device itself. In hybrid graphene-waveguide structures, graphene can affect the evanescent field of guided optical modes and reduce the absorption length of the waveguide device compared to the systems without graphene integration. The absorption within the device will vary depending on the numbers of the integrated graphene layers. Li et al. have transferred a single layer graphene onto a photonics substrate using the technique presented in reference [20]. A single layer graphene was grown on a copper foil by using the chemical vapor deposition (CVD). Wang J et al. [33], have presented the graphene-on-silicon slot waveguide structure, where absorption analysis is performed in TE and TM modes for both silicon waveguide and the graphene layer which has a fixed thickness of 0.7 nm. In this study, the thickness of the monolayer graphene was fixed, where the photodetection application has been developed based on improved responsivity. In reference [34] the author presented a graphene-on-silicon (GoS) suspended vertical slot waveguide, in which they have performed both refractive index and phase shifting by

* Corresponding author at: Computational Optics Research Group, Advanced Institute of Materials Science, Ton Duc Thang University, Ho Chi Minh City, Viet Nam.
E-mail address: irajsadeghamiri@tdt.edu.vn (I.S. Amiri).
URL: https://scholar.google.com.my/citations?user=rM8jFG4AAAAJ&hl=en (I.S. Amiri).

https://doi.org/10.1016/j.rinp.2018.04.020
Received 19 March 2018; Received in revised form 8 April 2018; Accepted 9 April 2018
Available online 13 April 2018

modifying the Fermi level of the fixed graphene layer. By applying the voltage 1.5 to 3 V based on an electro-optic modulator, the Fermi level of the graphene layer could be changed from 0.4 to 2 eV. This change performed due to the strong interaction of propagating light with the graphene layer. Different waveguide structures such as Mach–Zehnder interferometer (MZI) and microring modulators were designed. In [35] a similar study is presented based on a plasmonic application, where the slot waveguide's width varies within the rib/slot waveguide design. The Fermi level of the graphene sheet deposited on top of the waveguide was changed by the electro-optic effect from 0 to 0.5 eV. Therefore for the Fermi level of 0.3 eV and higher, the surface plasmon polariton (SPP) is excited in the graphene sheet. The excited SPP field further is distributed within the adjustable slot and has caused optical losses in the waveguide changes according to different widths of the slot. In this study the geometric tunability of the optical propagation losses of the waveguide and transmission spectrum monitoring were performed, where graphene sheet thickness was fixed at 0.7 nm. In our study, we have further investigated the optical transmissivity of the silicon waveguide provided the graphene layer thickness varies between 0.38 and 3800 nm. In the hybrid graphene-waveguide devices, the geometry and mode profiles can be engineered in such a way that the electric field propagation within the graphene can be controlled. High absorption property of the graphene can be utilized to build up new sensing devices based on graphene-waveguide configurations with a small footprint and high efficiency, high speed, broadband photodetection and efficient modulation [36].

The straight silicon waveguide is utilized, where the substrate material is SiO_2 with 4 μm thickness. On the top of SiO_2, silicon channel as a waveguide has 180 nm thickness and width of 475 nm. Changing the thickness of graphene which is sandwiched between two straight waveguides can influence the propagation of light. Graphene film owing to its weak interforce van der Waals interaction between the sheet (monolayer) of carbon atoms which can contain one sheet, several sheets or several thousand sheets within its structure. The optical and electronic properties of multilayer graphene are sensitive to the number of layers as well as the stacking sequence [9,37,38]. Considering a graphene layer composed of one atomic layer (Fig. 1a) or multiple atomic layers (Fig. 1b) allocates within two micro-scale sections of silicon waveguide as shown in Fig. 1.

By adding more monolayer of graphene, basically, it would tend to block the propagation of light. Thus, a graphene's grate with different length (or a number of a monolayer) plays a deterministic role to control the confined power within the structure of joint silicon waveguides with the graphene's grate as an interface layer.

Arbitrary geometric complexity, such as the nonlinear least squares and curves can be solved by FDTD method which is a multipurpose and precise method for simulating light propagation in the scale of nanocomponents [39–42]. 2.5D variational FDTD (varFDTD) method can be used for planar geometries and it is a way to make the simulation function that can provide high accuracy in comparison to 3D FDTD. This method can make the computation times similar to 2D FDTD. The varFDTD method is particularly suitable for the primary optimization stage and offers a very efficient way to achieve an estimated optimal state [43]. The updating equation for the H-field along the z-direction reads

$$H_z^{n+1/2}(i,j,k) = H_z^{n-1/2}(i,j,k) + \frac{\Delta t}{\mu * Area(i,j,k)} \times \{E_x^n(i,j,k) * d_x(i,j,k) - E_x^n(i,j-1,k) d_x(i,j-1,k) - E_y^n(i,j,k) d_y(i,j,k) + E_y^n(i-1,j,k) d_y(i-1,j,k) \quad (1)$$

In Eq. (1), d_x and d_y are cell lengths along the x and y directions, respectively. Using adjacent H-field values, the E-field can be updated in a conventional manner provided the H-field has been computed. Following equation shows the derivation of the updated E-field along the x-direction.

$$E_x^{n+1}(i,j,k) = E_x^n(i,j,k) + \frac{\Delta t}{\varepsilon \times \Delta y}\{H_z^{n+1/2}(i,j+1,k) - H_z^{n+1/2}(i,j,k)\} - \frac{\Delta t}{\varepsilon \times \Delta z}\{H_y^{n+1/2}(i+1,j,k) - H_y^{n+1/2}(i,j,k)\} \quad (2)$$

In Eq. (2), Δy and Δz are the step size along y and z directions. The specifications of the mesh are not demanding, therefore, automatic mesh generation procedure has been utilized in conjunction with the presented algorithm [44]. In order to perform the characterization on graphene layers and required calculations, the density functional theory (DFT) has been utilized. To calculate the complex graphene refractive index and dielectric constant, the Vienna Ab-initio simulation has been utilized for both in-phase (xx) and cross-plane (zz) directions. At first, the charge density distributions were calculated to use in the dielectric function calculations and electronic band structure. This calculation provides RIG = 2.71 + 1.41i [45].

Result and discussions

Modeling results of the transmission behavior of the light propagating within the silicon waveguide with cross-sectional dimensions of 475 nm width and of 180 nm thickness are discussed in this section. As can be seen in Figs. 2(a)–7(a), the optical axis of silicon waveguide is in the x-direction with a length of 10 μm. Fig. 2(a)–(c) show reference figures and are emphasizing on the situation if the graphene grate is not defined within the waveguide structure. It must be noted that the white dashed line in Figs. 2(a)–7(a) demonstrates the x coordinate location of silicon waveguide's aperture (i.e. the point (x = −4.8) where the light beam as the source injects maximum power to the waveguide). Despite of insignificant variation of the power over the wavelength range of 1.5 $\mu m - 1.6$ μm (Fig. 2c), it can be seen from Fig. 2b, silicon waveguide perfectly confined 100% of the power over this range.

Now, we assume that a monolayer of graphene grate (red dash line in Fig. 3a) with complex refractivity is used base on DFT method [46] as an interface layer blocking the propagating waves along the optical

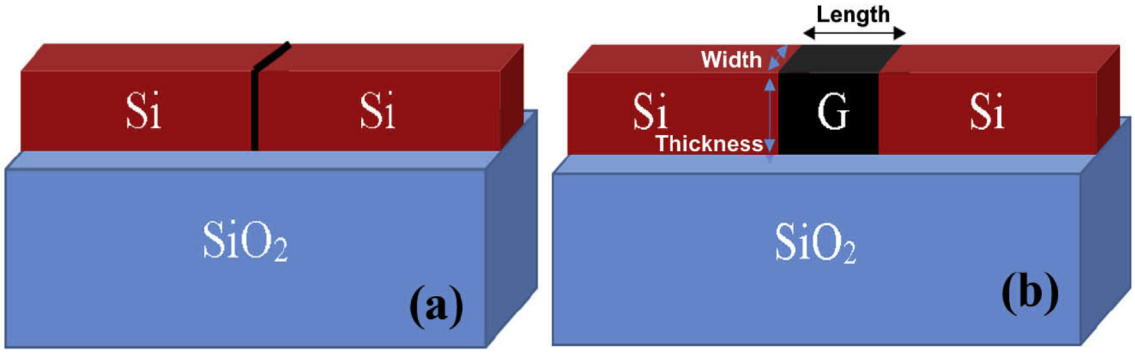

Fig. 1. (a) Schematic of silicon optical waveguides associate with a single atomic layer of Graphene, (b) multiple atomic layers of graphene.

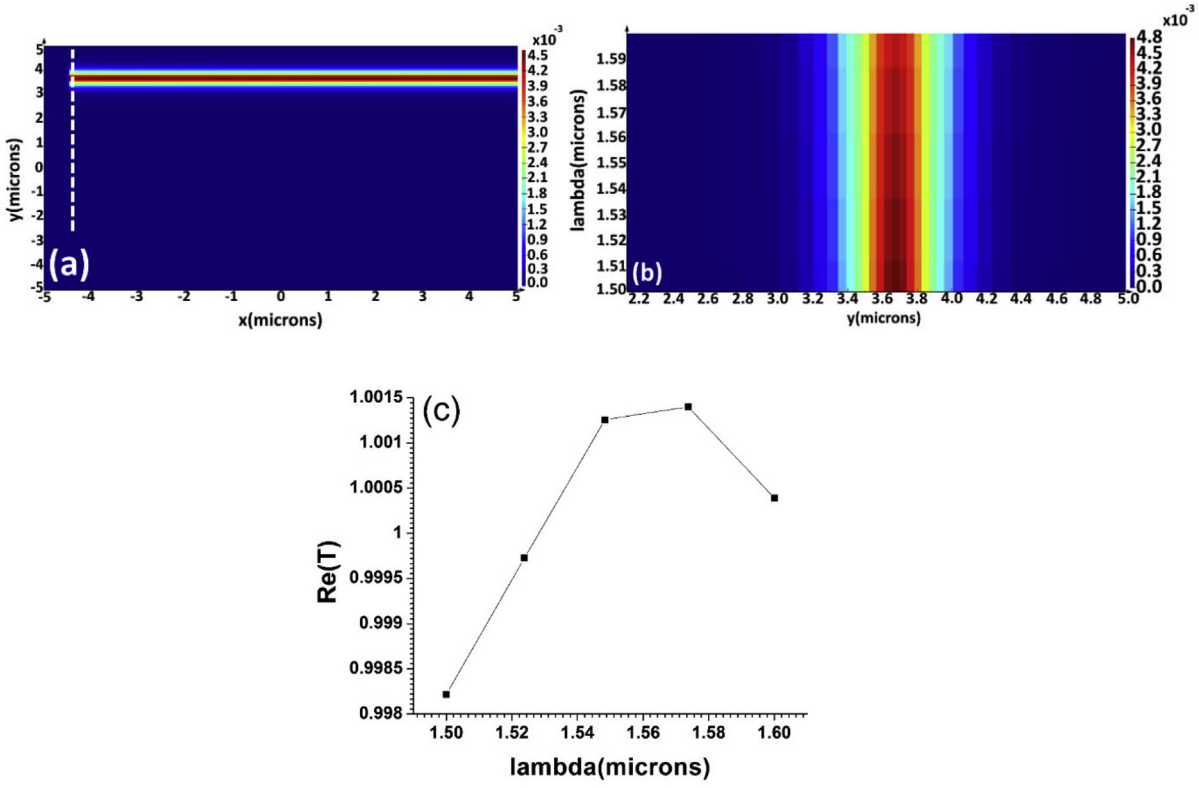

Fig. 2. (a) Top view of the optical power propagating in the silicon waveguide in the non-existence of graphene grate, (b) power profile of silicon waveguide, (c) power spectrum.

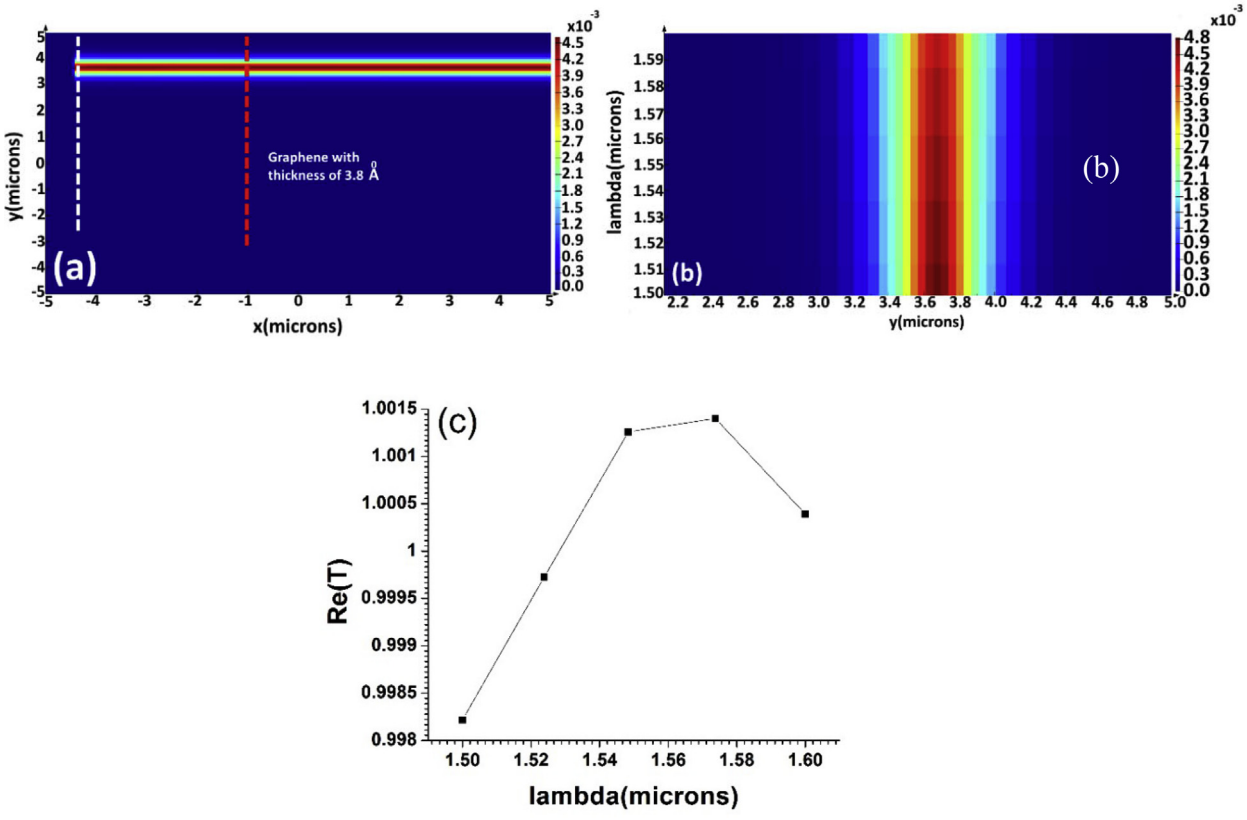

Fig. 3. (a) Top view of the optical power propagating in the silicon waveguide in the existence of mono-layer graphene grate 3.8 Å (or 0.38 nm), (b) power profile, (c) power spectrum.

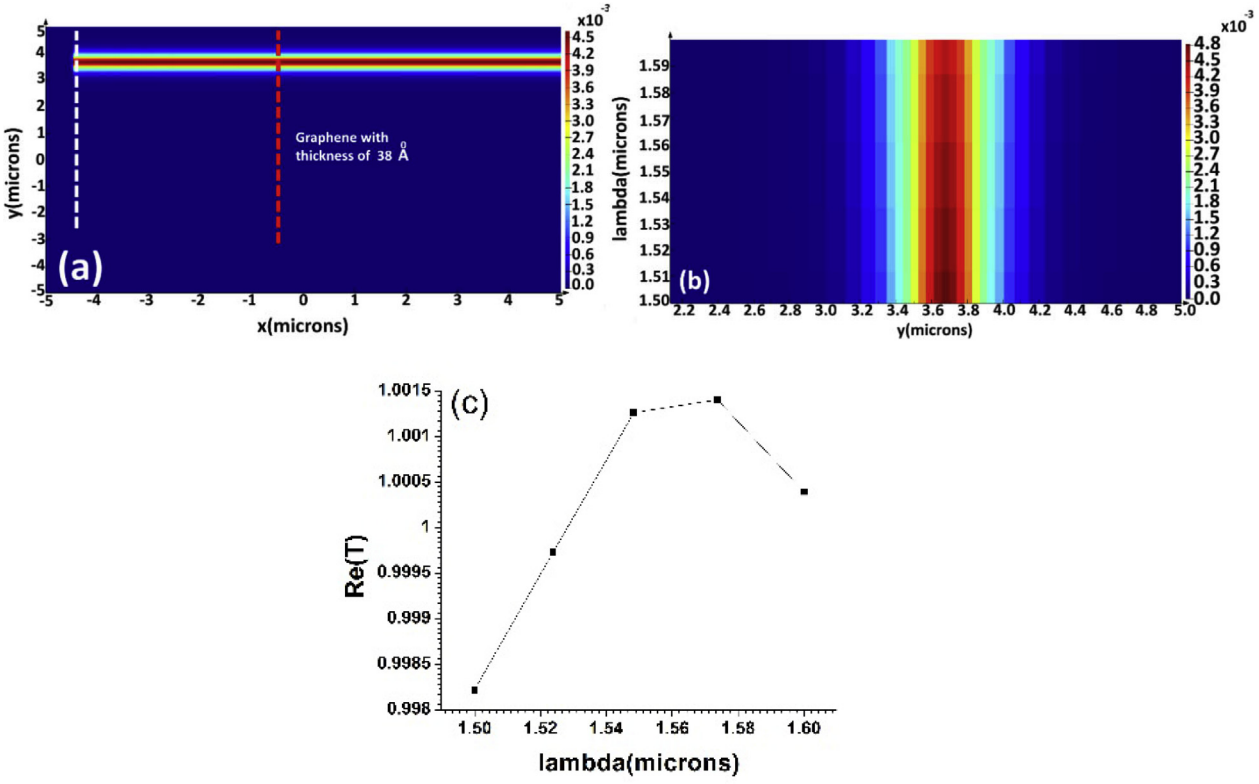

Fig. 4. (a) Top view of the optical power propagating in the silicon waveguide in the existence of multi-layer graphene grate 38 Å (or 3.8 nm), (b) Power profile of silicon waveguide after graphene layer, (c) power spectrum of the silicon waveguide.

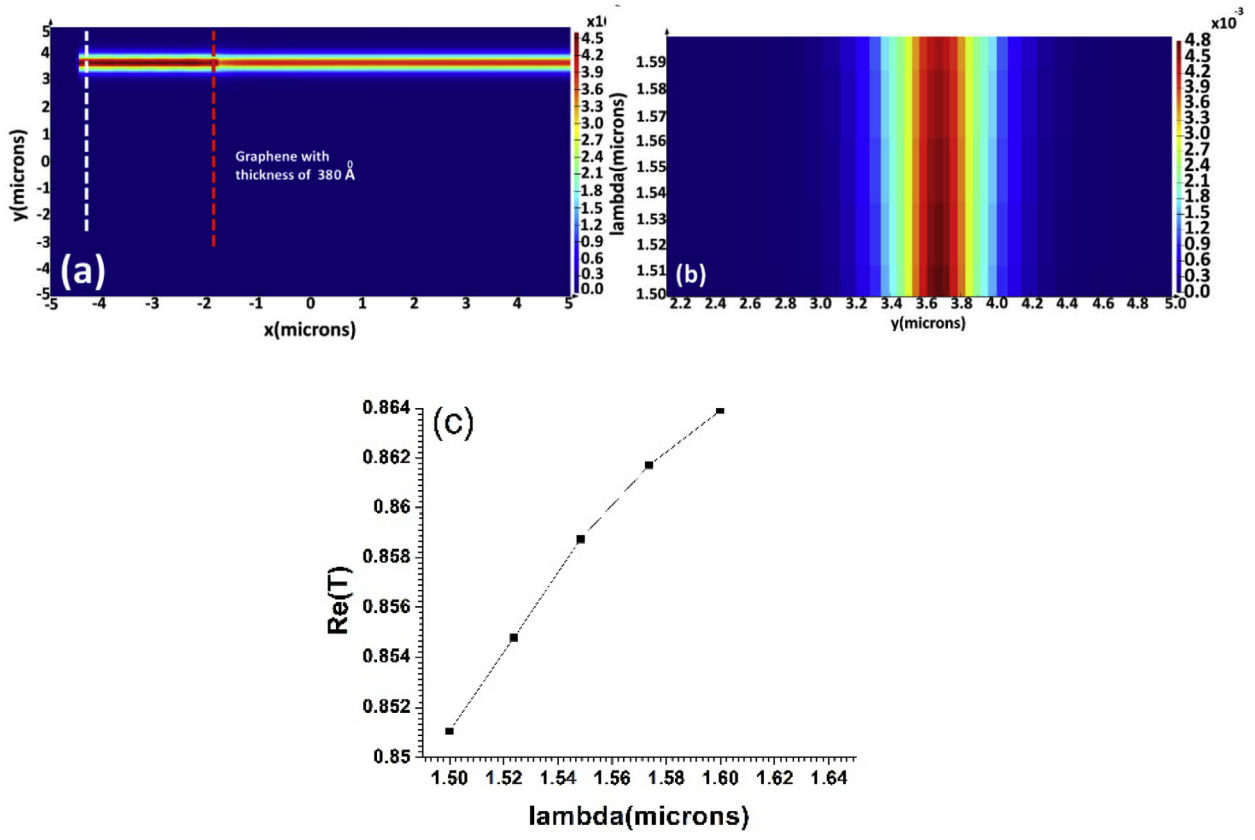

Fig. 5. (a) Top view of the optical power propagating in the silicon waveguide in the existence of multi-layer graphene grate 380 Å (or 38 nm), (b) power profile, (c) power spectrum.

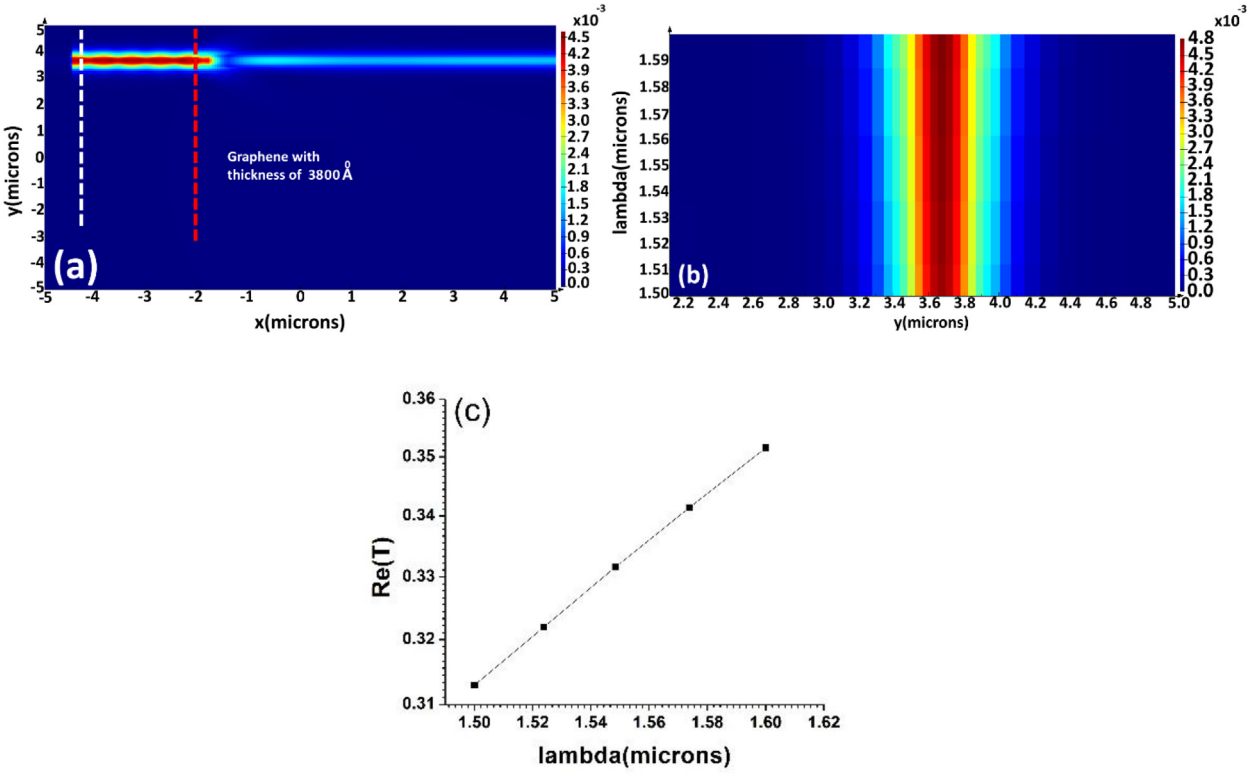

Fig. 6. (a) Top view of the optical power propagating in the silicon waveguide in the existence of multi-layer graphene grate 3800 Å (or 380 nm), (b) power profile, (c) power spectrum.

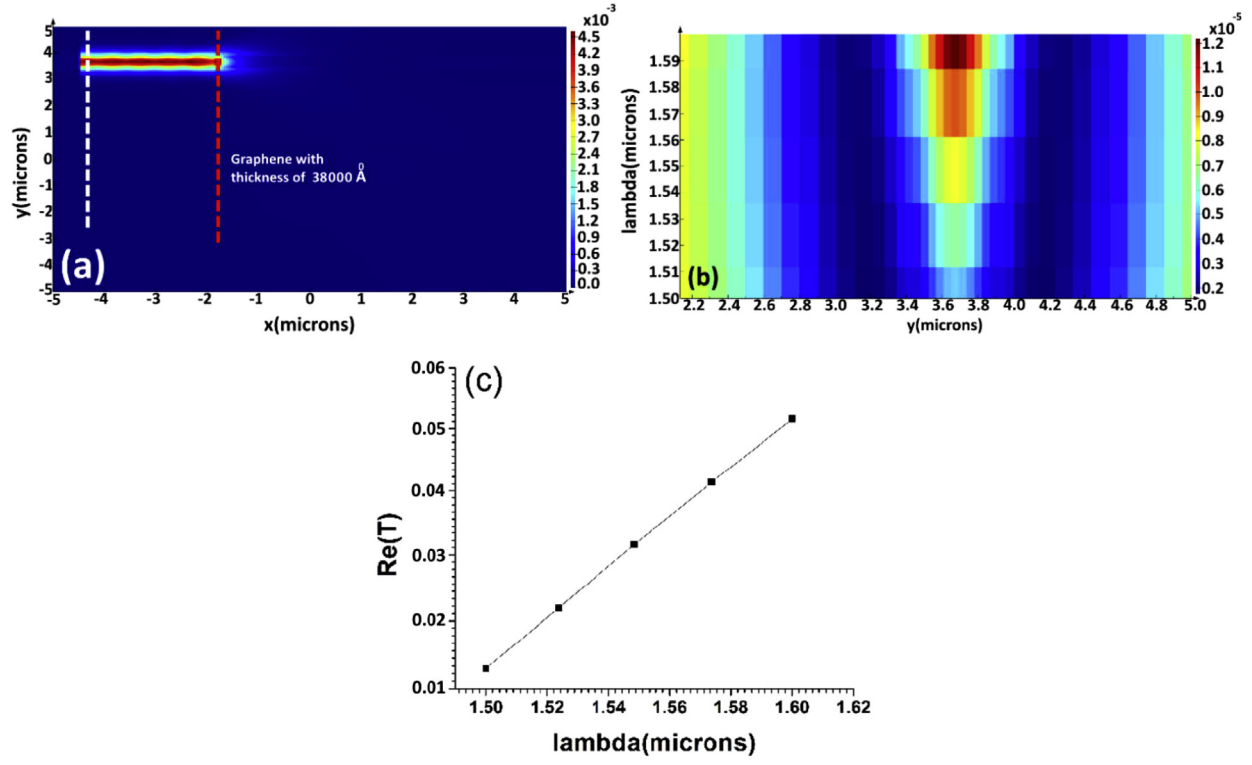

Fig. 7. (a) Top view of the optical power propagating in the silicon waveguide in the existence of multi-layer graphene grate 38000 Å (or 3800 nm), (b) power profile, (c) power spectrum.

axis. Within the context, the best transmissivity of graphene can be obtained at the length of 3.8 Å (or 0.38 nm). Introducing one atomic size layer of graphene as an interfacing layer between two sections of a silicon waveguide would not have an impact on the power profile and the spectrum as shown in Fig. 3b and c.

Basically, the absorptivity of the graphene grate will increase with the increase of atomic layers. In Fig. 4 the modeling investigates the situation of light transmissivity in silicon waveguide under the condition of using graphene that is 10 times thicker 38 Å (or 3.8 nm). Regardless of the structural variation of graphene grate, spectral results shown in Fig. 4b and 4c still do not indicate a sensible change in power and spectrum profiles compare with the situations studied in Figs. 2 and 3.

The graphene length of 100 times longer than monolayer graphene affords semi-blocking, property, either in optical power plot (Fig. 5a) or spectral plots (Fig. 5b and c) of the proposed silicon waveguide in this study. The transmissivity in this situation has reduced from 100% to about 80% as can be observed in Fig. 5c which is expected with larger number of Graphene monolayers. Now, our special emphasis is on transmissivity at a longer length of graphene grate.

The input power is a wavelength band within the range of 1.5 to 1.6 μm, where the center wavelength has been selected to 1.57 μm. Increasing the graphene thickness (38 nm and greater) will affect the power transmissions as the center wavelength will have a red shift toward longer wavelengths. In Figs. 6 and 7 the peaks of the transmission spectrum have shifted to longer wavelengths. Fig. 6 shows that the minor portion (~% 30 as to Fig. 6c) of the power can still transmit even at 1000 atomic layers of graphene.

Fig. 7 illustrates that by further increasing the graphene thickness equivalent to around 10,000 layers, 38000 Å (or 3800 nm), the light beam is almost completely blocked allowing only less than 1% transmission through the graphene grate into the silicon waveguide.

In summary, the transmissivity of light with the influence of graphene layers is investigated. The graphene integrated into the silicon waveguide has light blocking effects which depend on the number of its layers as the layers increase the transmission is reduced through the waveguide length, where graphene with fewer layers allows a portion of the light to pass through the length depending on the number of its atomic layer.

Conclusion

This study addresses the transmissivity limitations posed by introducing graphene layers with different number atomic layers as an interface layer between two sections of a silicon waveguide. Based on the achievements, the highest transmissivity of the power (~100%) within the waveguide can be obtained if the number of atomic layers being less than 100 (38 nm). Assuming the number of atomic layers changes between 100 and 1000 atomic layers (or 380 nm and 3800), the transmitted power varies in the range between ~80% and ~30%. Light is blocked to ~99% of at 10,000 (or 38,000) atomic layers of the graphene grate.

References

[1] Amiri I, et al. All-Optical Generation of Two IEEE802.11n Signals for 2 × 2 MIMO-RoF via MRR System. IEEE Photonics J 2014;6(6):1–11.
[2] Teeka, C., et al. ASK-to-PSK Generation based on Nonlinear Microring Resonators Coupled to One MZI Arm. In: AIP Conference Proceedings, 2011. AIP.
[3] Soltanian MRK, et al. Dual-wavelength erbium-doped fiber laser to generate terahertz radiation using photonic crystal fiber. J Lightwave Technol 2015;33(24):5038–46.
[4] Soltanian M, et al. A simple humidity sensor utilizing air-gap as sensing part of the Mach-Zehnder interferometer. Opt Quant Electron 2017;49(9):308.
[5] Soltanian M, et al. Variable Waist-Diameter Mach-Zehnder Tapered-Fiber Interferometer as Humidity and Temperature Sensor. IEEE Sens J 2016;16(15):5987–92.
[6] Novoselov KS, et al. Electric field effect in atomically thin carbon films. Science 2004;306(5696):666–9.
[7] Zhang Y, et al. Experimental observation of the quantum Hall effect and Berry's phase in graphene. Nature 2005;438(7065):201.
[8] Bonaccorso F, et al. Graphene photonics and optoelectronics. Nat Photonics 2010;4(9):611–22.
[9] Avouris P. Graphene: electronic and photonic properties and devices. Nano Lett 2010;10(11):4285–94.
[10] Ahmad H, et al. Gold cone metasurface MIC sensor with monolayer of graphene and multilayer of graphite. Plasmonics 2017;12(2):497–508.
[11] Amiri IS, et al. Vertical Ge photodetector base on InP taper waveguide. Results Phys 2018.
[12] Kuzmenko A, et al. Universal optical conductance of graphite. Phys Rev Lett 2008;100(11):117401.
[13] Stauber T, Peres N, Geim A. Optical conductivity of graphene in the visible region of the spectrum. Phys Rev B 2008;78(8):085432.
[14] Wang F, et al. Gate-variable optical transitions in graphene. Science 2008;320(5873):206–9.
[15] Li Z, et al. Dirac charge dynamics in graphene by infrared spectroscopy. Nat Phys 2008;4(7):532–5.
[16] Vasko F. Saturation of interband absorption in graphene. Phys Rev B 2010;82(24):245422.
[17] Bolotin KI, et al. Ultrahigh electron mobility in suspended graphene. Solid State Commun 2008;146(9):351–5.
[18] Gannett W, et al. Boron nitride substrates for high mobility chemical vapor deposited graphene. Appl Phys Lett 2011;98(24):242105.
[19] Li X, et al. Large-area synthesis of high-quality and uniform graphene films on copper foils. Science 2009;324(5932):1312–4.
[20] Li X, et al. Transfer of large-area graphene films for high-performance transparent conductive electrodes. Nano Lett 2009;9(12):4359–63.
[21] Novoselov K, et al. Two-dimensional gas of massless Dirac fermions in graphene. Nature 2005;438(7065):197–200.
[22] Amiri I, Ariannejad M, Ahmad H. Tunable multi-wavelength generation using InGaAsP/InP microring resonator with detectable resonance wavelength shift due to a sensing cladding section. Chin J Phys 2016;54(5):780–7.
[23] Kim K, et al. A role for graphene in silicon-based semiconductor devices. Nature 2011;479(7373):338–44.
[24] Shakeri M, et al. Advanced cmos based image sensors. Aust J Basic Appl Sci 2012;6(7):62–72.
[25] Bao Q, et al. Broadband graphene polarizer. Nat Photonics 2011;5(7):411–5.
[26] Bao Q, et al. Atomic-layer graphene as a saturable absorber for ultrafast pulsed lasers. Adv Funct Mater 2009;19(19):3077–83.
[27] Amiri, IS, et al. Microring resonator made by ion-exchange technique for detecting the CO2, H2O, and NaCl as cladding layer. J King Saud Univ-Sci, 2017.
[28] Amiri IS, et al. Simulation of microring resonator filters based ion-exchange buried waveguide using nano layer of graphene. J Opt 2017;46(4):506–14.
[29] Amiri I, et al. Visible Wireless Communications Using Solitonic Carriers Generated by Microring Resonators (MRRs). Iran J Sci Technol Trans A Sci 2016:1–7.
[30] Amiri I, Ali J. Optical quantum generation and transmission of 57–61 GHz frequency band using an optical fiber optics. J Comput Theor Nanosci 2014;11(10):2130–5.
[31] Gaskell P, et al. Counting graphene layers on glass via optical reflection microscopy. Appl Phys Lett 2009;94(14):143101.
[32] Ariannejad MM, et al. Design of an 8-cell dual port SRAM in 0.18-μm CMOS technology. Res J Appl Sci Eng Technol 2013;5(8):2565–8.
[33] Wang J, et al. High-responsivity graphene-on-silicon slot waveguide photodetectors. Nanoscale 2016;8(27):13206–11.
[34] Phatak A, et al. Design of electro-optic modulators based on graphene-on-silicon slot waveguides. Opt Lett 2016;41(11):2501–4.
[35] Xiao T-H, Cheng Z, Goda K. Graphene-on-silicon hybrid plasmonic-photonic integrated circuits. Nanotechnology 2017;28(24):245201.
[36] Li H, et al. Optical absorption in graphene integrated on silicon waveguides. Appl Phys Lett 2012;101(11):111110.
[37] Nair RR, et al. Fine structure constant defines visual transparency of graphene. Science 2008;320(5881). 1308-1308.
[38] Katsnelson MI, Katsnel'son MI. Graphene: carbon in two dimensions. Cambridge University Press; 2012.
[39] Amiri I, et al. Increment of access points in integrated system of wavelength division multiplexed passive optical network radio over fiber. Sci Rep 2015;5:11897.
[40] Amiri I, et al. Multi wavelength mode-lock soliton generation using fiber laser loop coupled to an add-drop ring resonator. Opt Quant Electron 2015;47(8):2455–64.
[41] Amiri I, Naraei P, Ali J. Review and theory of optical soliton generation used to improve the security and high capacity of MRR and NRR passive systems. J Comput Theor Nanosci 2014;11(9):1875–86.
[42] Soltanian M, et al. A stable dual-wavelength Thulium-doped fiber laser at 1.9 μm using photonic crystal fiber. Sci Rep 2015;5.
[43] Ma Y, et al. Ultralow loss single layer submicron silicon waveguide crossing for SOI optical interconnect. Opt Exp 2013;21(24):29374–82.
[44] Dey S, Mittra R. A locally conformal finite-difference time-domain (FDTD) algorithm for modeling three-dimensional perfectly conducting objects. IEEE Microwave Guided Wave Lett 1997;7(9):273–5.
[45] Cheon S, et al. How to reliably determine the complex refractive index (RI) of graphene by using two independent measurement constraints. Sci Rep 2014;4.
[46] Klintenberg M, et al. Evolving properties of two-dimensional materials: from graphene to graphite. J Phys Condens Matter 2009;21(33):335502.